Heliyon 5 (2019) e02256

Contents lists available at ScienceDirect

Heliyon

journal homepage: www.heliyon.com

Evaluation of water absorption and chloride ion penetration of rice straw ash and microsilica admixed pavement quality concrete

Arunabh Pandey *, Brind Kumar

Department of Civil Engineering, Indian Institute of Technology (Banaras Hindu University), Varanasi, 221005, India

ARTICLE INFO

Keywords:
Civil engineering
Construction engineering
Concrete technology
Cement additive
Concrete structure
Cement
Rice straw ash
Microsilica
Air content
Water absorption
Chloride ion penetration

ABSTRACT

The effects of rice straw ash (RSA) and microsilica (MS) on durability properties (water absorption and chloride ion penetration) of M40 grade Pavement Quality Concrete (PQC) were studied. Ten concrete samples were prepared by partially substituting cement with RSA and MS in various proportions. A significant reduction was observed in the water absorption and chloride ion penetration in concrete samples with an increase in the curing age as well as with an increase in the proportion of MS and RSA. The maximum reduction in water absorption and chloride ion penetration was observed in R2M3 (10% RSA and 7.5% MS) as compared to control concrete (R0). The analytical relationships were developed between the above-mentioned parameters and curing age of concrete. A linear equation was established between the initial and secondary rate of water absorption of concrete and also between the chloride ion penetration of concrete at 10–20 mm and 25–35 mm depth. Both these equations were applicable to all the concrete samples of this study. Predictive charts were generated between the above-mentioned parameters and days of curing in water.

1. Introduction

The cement industries have caused severe damage to the environment. They are one of the primary sources of CO_2 emission into the atmosphere and account for nearly 5% of the global emission [1]. Various studies have confirmed that mineral admixtures can be used to replace cement in concrete partially. Mineral admixtures improve the mechanical as well as durable properties of the concrete. Microsilica has been the leading mineral admixture used in high strength concrete [2, 3, 4].

Rice straw is one of the major by-products of agriculture. The rice straw production in Asia per year is approximately 95% of the total production in the entire world [5]. In India, rice straw is the leading agro-residue produced [6]. The RSA (ash produced when the rice straw is burnt) can be reused as a pozzolanic supplementary material in cement due to its high silica (SiO_2) content [7, 8, 9, 10, 11, 12].

The durability properties of the concrete mainly depend on its curing age among the other factors. Porosity and chloride ion penetration of concrete decreases with increase in the curing age [13]. It is due to an increase in the amount of C-S-H gel, which ties together the cement particles into a firm entity [14]. The addition of mineral admixtures improves the durability properties of concrete because of the finer size of their particles as compared to the cement particles. The space left after the process of hydration is filled by the finer particles leading to the densification of the microstructure. This densification also improves the Interfacial Transition Zone (ITZ) [15]. The formation of extra C-S-H gel as a result of the reaction between calcium hydroxide (from hydration reaction) and silica (from the mineral admixtures) also enhances durability properties of concrete [16]. As the particle size of the RSA was found to be less than the size of cement particles, it may lead to improved durability properties of concrete [17].

Few researchers in the past have observed the effects of RSA on the primary and mechanical properties of cement paste, mortar and concrete [8, 9, 10, 17, 18]. But the effect of RSA on the durability properties of concrete has not been addressed in the past. Therefore, the principal purpose of this study was to observe the effect of RSA (with or without MS) on durability properties of M40 grade PQC.

2. Materials and methods

2.1. Materials and mix design

The combination of Grade 43 OPC (Ordinary Portland Cement), RSA and MS constituted the binder content in the concrete. Grade 920D MS and rice straw were obtained from Elkem South Asia Pvt Ltd and

* Corresponding author.
E-mail address: arunabh.rs.civ13@iitbhu.ac.in (A. Pandey).

https://doi.org/10.1016/j.heliyon.2019.e02256
Received 18 March 2019; Received in revised form 15 April 2019; Accepted 5 August 2019

Table 1
Phase composition of cement, rice straw ash, and microsilica.

material	compound, % by wt														
	SiO_2	CaO	MgO	Al_2O_3	Fe_2O_3	P_2O_5	SO_3	Na_2O	SrO	Cl	TiO_2	S	K_2O	P	ZnO
cement	20.34	62.16	0.79	6.13	3.7	2.03	1.73	1.33	0.45	0.305	0.189	-	-	-	-
RSA	79.82	0.370	7.54	1.13	0.245	3.75	-	0.501	-	4.06	-	1.16	1.07	-	-
MS	91.3	0.171	1.29	0.616	1.47	-	3.13	0.082	-	-	-	-	0.653	0.38	0.244

Table 2
Details of mix proportions & HRWR dosage.

material	mix proportion, % by wt									
	R0 or control	R2	M1	M2	M3	M4	R1M2	R1M3	R2M2	R2M3
OPC	100	90	97.5	95	92.5	90	90	87.5	85	82.5
RSA	-	10	-	-	-	-	5	5	10	10
MS	-	-	2.5	5	7.5	10	5	7.5	5	7.5
HRWR[a]	0.4	1.5	0.9	1.05	1.2	1.3	1.7	2	2.4	2.5

[a] HRWR dosage was in % by weight of binder material (OPC + RSA + MS).

agricultural farm of Banaras Hindu University, India respectively. MS was used in concrete as was supplied while production of RSA from the burning of rice straw was as per the previous study by the authors [17]. The detailed investigation about the reactivity of RSA was also done in the past by the authors, which supported the use of RSA as a mineral admixture [7]. The specific surface area of the OPC, RSA and MS was 0.3, 1.846 and 16.14 m^2/g respectively while the mean grain size of the same was 17, 3,3 and 0.6 μm respectively. The phase composition of cement, microsilica and rice straw ash as obtained in the previous work by the authors is shown in Table 1 for a better understanding of the results of the present investigation [17]. The high amount of SiO_2 in MS as well as in RSA justifies their usage as a mineral admixture.

The coarse aggregates (20 mm and 10 mm nominal size), as well as fine aggregates, were obtained from two different quarries in Sonebhadra, Uttar Pradesh, India. The water absorption and specific gravity of fine aggregates were 1.1% and 2.65 respectively. The crushing, as well as impact value of the coarse aggregates, were 10.6% and 9.5% respectively. 20 mm size coarse aggregates had the water absorption and the specific gravity of 0.6% and 2.78 respectively while the same for 10 mm size coarse aggregates were 0.75% and 2.72 respectively.

The final concrete mix design was as per IRC 44 and IS 10262 [19,20]. As per the mix design of concrete, the quantities of materials used per m^3 of concrete were 755.91 kg of 20 mm size coarse aggregate, 493.06 kg of 10 mm size coarse aggregate, 663.87 kg of fine aggregate and 406 kg of total binder content. The water to binder ratio (w/b) was 0.39. As w/b ratio was fixed, the decrease in workability due to the incorporation of RSA and MS in concrete was compensated by the usage of sulphonated naphthalene polymer-based high range water reducer (HRWR). Conplast SP430 HRWR was procured from Fosroc Chemicals (India) Pvt Ltd. The dosage of HRWR in each concrete mix was decided by slump test of concrete as per ASTM C143 [21]. The amount of HRWR required to maintain the slump at 50 mm for each concrete mix is shown in Table 2.

Based on the previous study by the authors [18], only mix R2 (90% OPC, 10% RSA) was selected for investigating the effects of RSA on water absorption and chloride ion penetration in concrete. The mix proportions which were finalized for admixed concrete having a target cube compressive strength of 40 MPa at 28 days of curing are given in Table 2.

2.2. Experimental methodology

The experiment to obtain air entrainment in fresh concrete was performed by pressure method as per ASTM C173 [22]. Fig. 1 shows the experimental setup of measuring air entrainment in fresh concrete.

All the samples of concrete were cast and left covered for 24 hours in the casting room. Following 24 hours of casting, the samples were removed from the mould and placed in the water curing tank as per ASTM C192 [23]. The samples were subjected to 3, 7, 28, 60, 90 and 365 days of curing until the time of testing. The curing water was restored after every 7 days. The temperature of curing water was maintained at $27^o \pm 2$ °C. Three samples of concrete were cast for every mix designation after each day of curing, and the average of the three values after the respective curing age was reported for every test.

Fig. 1. Setup for air entrainment of fresh concrete test.

For a saturated water absorption test, concrete cubes of size 15 cm were cast for every mix designation after each day of curing. It was measured as per ASTM C642 [24].

For the rate of water absorption test and coefficient of water absorption test, concrete cylinders (10 cm dia. & 20 cm height) were cast for every mix designation, and the test was performed as per ASTM C1585 [25]. After curing, the specimens were dried in an oven at 50 °C for 3 days. They were then sealed in a chamber at 23 °C for 15 days. After 15 days, the side and top surface of the concrete cylinders were covered with a polythene sheet. The polythene sheet was tightened in place by a flexible cord and water-proof duct tape. The bottom surface of the cylinders was left uncovered to permit the movement of water in one direction only. The initial mass of the prepared sample was taken. They

Fig. 2. Configuration for the rate of water absorption and coefficient of water absorption test.

were submerged in the water to the extent of 3 mm from the bottom surface on porcelain rods, as shown in Fig. 2. The mass of absorbed water by the prepared specimens was taken at specified intervals (1, 5, 10, 20, 30 and 60 minutes; 2, 3, 4, 5 and 6 hours; 1, 2, 3, 4, 5, 6 and 7 days). The mass of water absorbed (M) at time T, the open surface area of sample (A), and density of water (D) were obtained to calculate the rate of water absorption (I) as per the Eq. (1). According to ASTM C1585 [25], the slope of the line best fit to 'I' plotted against the square root of time 1, 5, 10, 20, 30 and 60 minutes was taken as the initial rate of water absorption and against the square root of time 1, 2, 3, 4, 5, 6 and 7 days was taken as the secondary rate of water absorption.

$$I = M/(A*D) \quad (1)$$

The chloride ion penetration test of concrete slabs (300 mm^2 & 75 mm thickness) of every mix was conducted as per ASTM C1543 [26]. The sides of the slab were covered with closed-cell polystyrene foam, and the bottom surface was left uncovered for proper circulation of air. The polystyrene foam was held together by water-proof duct tape. A rapid-setting epoxy adhered to the vertical surface of polystyrene foam and the horizontal surface of the slab for water-proofing. The ponding solution (3% reagent grade NaCl by weight in water) was maintained up to 2 cm, as shown in Fig. 3. The top surface was capped with a glass film to avoid excessive dissipation of water through evaporation from the ponding solution. After 90 days of ponding, the NaCl solution was removed, and the surface of the slab was left to dry. The salt crystals formed on the surface of the slab were removed using the wire scrub. The powdered samples were procured from the depths of 10–20 mm and 25–35 mm from the top surface of the concrete slab, as shown in Fig. 4, and the chloride ion percentage was obtained as per ASTM C1152 [27].

3. Results and discussions

3.1. Material properties

RSA and MS particles were 5 and 28 times finer than the OPC particles, respectively. Due to the incorporation of fine particles of RSA and MS into concrete, better resistance of concrete to water absorption and chloride ion penetration could be expected. Rice straw ash fulfils the criteria of ASTM C618-78 [28] for class F pozzolan. The absence of calcium oxide (CaO) and the presence of SiO_2 signify the importance of MS and RSA as pozzolans.

Fig. 3. Configuration of the concrete slab during the ponding.

Fig. 4. Drilled holes of 10–20 mm and 25–35 mm depth for obtaining samples for chloride ion penetration test.

Since rice straw ash contains a high amount of SiO_2 (79.82%), it could be used as a source of silica in glass production [29]. β-wollastonite could also be produced from rice straw ash by the process of autoclaving and sintering due to the presence of a high amount of silica [30]. Addition of wollastonite improves the properties of concrete significantly [3, 31]. It was found in the literature that Si (Silicon), Mg (Magnesium), K (Potassium) and Ca (Calcium) are the main elements of sunflower husk ash due to which it is used as a raw material in the production of ceramic products [32]. Since the amount of Si, Mg, K and Ca in rice straw ash were similar to the sunflower husk ash; rice straw ash could also be used as a precursor in ceramic industries. Rice straw ash also contains elements of K and Ca; therefore, it could also be used as a crude fertilizer to improve the properties of agricultural soil [33].

According to the literature, if the amount of magnesium oxide (MgO) in the cementitious material is more than 5%, the chances of cracking in concrete are higher [34]. The formation of magnesium hydroxide ($Mg(OH)_2$) due to the hydration of MgO increases the volume of the hardened and stable concrete matrix [35, 36]. This expansion in the volume of the concrete leads to the development of cracks. It could be one of the reasons for better performance of the microsilica admixed concrete as compared to rice straw ash admixed concrete as the MgO content in microsilica (1.29%) was less than the rice straw ash (7.54%).

3.2. Air entrainment of concrete

The air content in fresh concrete of every mix designation is shown in Table 3. The constant air content in fresh concrete was observed when OPC was partially replaced by 15% of more RSA and MS. The least air

Table 3
Air entrained in fresh concrete samples.

mix	R0	M1	M2	R2	M3	R1M2	M4	R1M3	R2M2	R2M3
air content, %	4.05	3.9	3.8	3.8	3.75	3.75	3.7	3.65	3.6	3.6

content was found in the concrete of mix R2M3 (3.6%). The researchers in the past observed that the HRWR does not significantly affect the air content in the fresh concrete [37]. They concluded that the effect of w/b ratio on the air content is higher than the effect of amount and type of mineral admixtures in the fresh concrete. As the w/b ratio was kept constant in this study, it can be deduced that the decline in the air content of the fresh concrete was because of incorporation of RSA and MS. Based on the literature, the decline could be attributed to the fibre-reinforcing effect of the rice straw ash particles and filler as well as pozzolanic effect of the microsilica particles.

Rigid pavements are subjected to freezing and thawing conditions in colder regions. They must be protected against freezing and thawing. Air entrainment is an essential segment of concrete mixtures exposed to freezing and thawing conditions [38]. When the maximum aggregate size of 20 mm is used in concrete, the air content of 3.5% in concrete under mild exposure is recommended [39]. As India is a tropical country, freezing and thawing do not pose a severe problem to rigid pavements except in few northern and north-eastern parts.

3.3. Saturated water absorption

The effect of long term curing on saturated water absorption of rice straw ash and microsilica admixed PQC can be seen in Table 4 and Fig. 5. It is evident from the results that the saturated water absorption of concrete of every mix designation reduces with the increase in the curing age. It could be attributed to a decrease in volume of permeable voids, as found in another study as well [40]. The saturated water absorption of concrete with rice straw ash and microsilica was lower as compared to the control concrete (R0). The reduction in saturated water absorption of concrete of mix designation M1, M2, R2, and M3 w.r.t. R0 was highest at three days of curing in water (10.79%, 12.83%, 15.50%, and 20.64% respectively). While the reduction in saturated water absorption of concrete of mix designation R1M2, R1M3, M4, R2M2, and R2M3 w.r.t R0 was highest at 365 days of curing in water (28.57%, 31.20%, 36.45%, 38.55%, and 40.65% respectively). The reduction in saturated water absorption of concrete was highest for mix designation R2M3 at all the days of curing in water. The rate of reduction in the saturated water absorption of MS admixed concrete was higher as compared to the RSA admixed concrete. It was because of the higher fineness and pozzolanic activity of the MS particles as compared to RSA particles. As particles of microsilica and rice straw ash were finer than the OPC particles; it led to the reorientation of the structure of concrete, thus resulting in the dense packing of the mix. Comparable discoveries were reported for concrete with fly ash and sugarcane bagasse ash [4]. The reduction in the saturated water absorption of the rice straw ash and microsilica admixed concrete was also because of the filler effect of RSA and MS particles. The addition of mineral admixtures optimizes the microstructure of the interfacial transition zone (ITZ) [40].

The power equations between curing age ('x' in days) and saturated water absorption ('y' in %) were developed by regression analysis with high correlation factor (R^2) as shown in Table 5.

3.4. Rate of water absorption

Table 6, Fig. 6 and Table 7, Fig. 7 show the initial and secondary rate of water absorption, respectively, of concrete of every mix designation. The reduction in the initial and secondary rate of water absorption of all the concrete specimens was observed with the increase in the curing age. After 28 days of curing, it can be seen that the initial rate of water absorption of concrete was higher for mix designation R0, M1, M2, R2, M3, and R1M2 as compared to mix designation R1M3, M4, R2M2, and R2M3. The change in the initial rate of water absorption of concrete was insignificant after 28 days of curing. It implies that the curing age (greater than 28 days) does not affect the initial rate of water absorption of admixed concrete. Thus it can be said that the 28 days curing age is crucial for PQC with RSA and MS. The initial rate of water absorption of concrete was lowest for mix designation R2M3 closely followed by mix designation R2M2. The percentage decrease in the initial rate of water absorption of concrete for mix designation R2M3 as compared to R0 was 58.24%, 50.89%, 30.68%, 37.30%, 34.44%, and 39.88% at 3, 7, 28, 60, 90 and 365 days of curing in water respectively.

The secondary rate of water absorption of concrete for mix designation R0, M1, M2, R2, and M3 decreased significantly until 28 days of curing and was found to be nearly constant thereafter. However, for concrete of mix designation R1M2, R1M3, M4, R2M2, and R2M3, the secondary rate of water absorption was almost constant after seven days of curing. The secondary rate of water absorption of concrete was lowest for mix designation R2M3 closely followed by mix designation R2M2. The percentage decrease in the secondary rate of water absorption of concrete for mix designation R2M3 as compared to R0 was 65.47%, 61.37%, 37.96%, 43.90%, 39.54%, and 44.47% at 3, 7, 28, 60, 90 and 365 days of curing in water respectively.

Interfacial transition zone (ITZ) which surrounds the aggregates has a higher water-cement ratio and fewer amounts of suspended cement particles as compared to the cement paste matrix. It results in higher porosity of the concrete without mineral admixtures. As the addition of MS and RSA improves the cementitious paste system around the aggregates, it led to a reduction in the w/b in ITZ. The filler and the pozzolanic effect of rice straw ash and microsilica reduces the preferred arrangement of C–S–H crystals [31]. That is why the rate of water absorption was lower for concrete with microsilica and rice straw as compared to control concrete. The percentage reduction in the initial rate of water absorption of concrete with an increase in the curing age was much higher as compared to the secondary rate of water absorption [41]. A similar study observed that the addition of mineral admixtures reduces the rate of water absorption of concrete as compared to the control concrete because

Table 4
Percentage of saturated water absorption of the admixed concrete.

curing age, days	mix designation									
	R0	M1	M2	R2	M3	R1M2	R1M3	M4	R2M2	R2M3
3	4.3	3.83	3.75	3.63	3.41	3.41	3.24	2.93	2.89	2.79
7	3.83	3.61	3.53	3.41	3.32	3.18	3.14	2.84	2.83	2.62
28	3.53	3.4	3.35	3.31	3.15	2.68	2.52	2.52	2.33	2.26
60	2.94	2.82	2.82	2.76	2.64	2.20	2.12	2.06	1.94	1.86
90	2.82	2.65	2.64	2.59	2.54	2.00	1.98	1.87	1.76	1.69
365	2.38	2.33	2.3	2.25	2.19	1.7	1.64	1.51	1.46	1.41

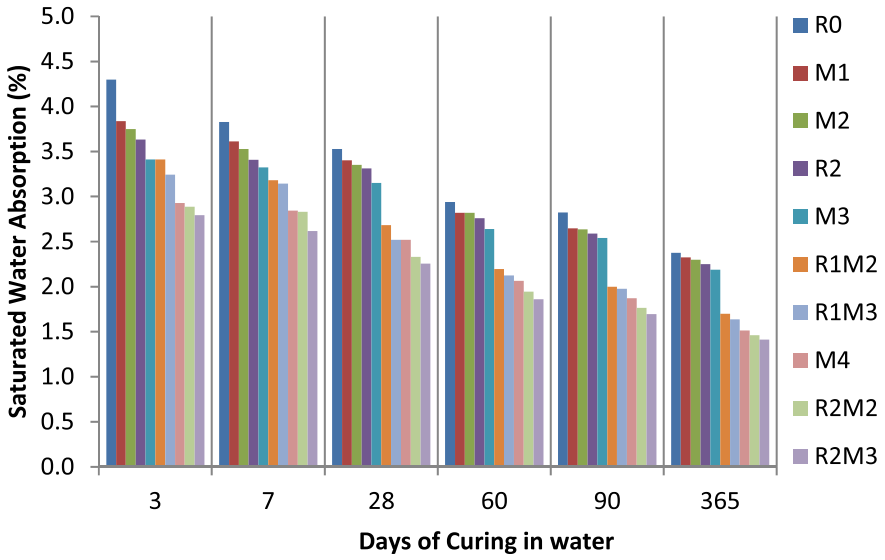

Fig. 5. Graph between Saturated water absorption of the admixed concrete & Days of curing in water.

Table 5
Mathematical relation between saturated water absorption and curing age.

mix designation	mathematical equation	R^2
R0	$y = 4.9702x^{-0.124}$	0.9757
M1	$y = 4.4695x^{-0.109}$	0.9447
M2	$y = 4.3502x^{-0.105}$	0.9428
R2	$y = 4.2088x^{-0.102}$	0.9253
M3	$y = 3.9775x^{-0.097}$	0.9271
R1M2	$y = 4.1918x^{-0.154}$	0.9761
R1M3	$y = 4.0278x^{-0.153}$	0.9802
M4	$y = 3.6778x^{-0.144}$	0.9458
R2M2	$y = 3.6319x^{-0.152}$	0.9682
R2M3	$y = 3.4336x^{-0.149}$	0.9732

Table 6
Initial rate of water absorption for admixed concrete (x 10^{-6} m/$s^{0.5}$).

mix	days of curing					
	3	7	28	60	90	365
R0	12.38	10.14	5.9	5.55	5.14	5.04
M1	11.48	9.79	5.62	5.29	5.13	4.97
M2	11.38	9.7	5.49	5.21	4.9	4.7
R2	9.51	9.01	5.36	5.15	4.65	4.42
M3	8.11	8.01	5.27	4.85	4.63	4.35
R1M2	8.04	7.63	5.24	4.76	4.48	4.17
R1M3	7.1	6.47	5.22	4.75	4.37	4.13
M4	6.98	5.75	5.22	4.73	4.29	3.9
R2M2	5.36	5.3	5.19	4.67	4.05	3.61
R2M3	5.17	4.98	4.09	3.48	3.37	3.03

of the densification of the cement paste [42]. But the addition of mineral admixtures also increases the chances of drying shrinkage because admixed concrete has little or no $Ca(OH)_2$ as most of it takes part in the formation of extra CSH gel. In the absence of $Ca(OH)_2$, C-S-H gel collapses due to the removal of water from the pore system leading to drying shrinkage of the admixed concrete. Therefore precautions should be taken while finalizing the proportion of mineral admixtures in the concrete.

The power equations between curing age ('x' in days) and the rate of water absorption ('y' in 10^{-6} m/$s^{1/2}$) were developed by regression analysis with high correlation factor (R^2) as shown in Tables 8 and 9.

The linear equations between the secondary rate of water absorption ('y' in 10^{-6} m/$s^{0.5}$) and the initial rate of water absorption ('x' in 10^{-6} m/$s^{0.5}$) were developed by regression analysis with very high correlation

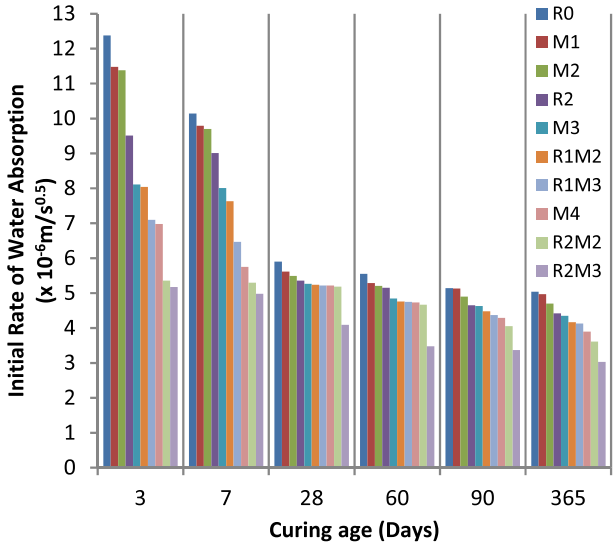

Fig. 6. Graph between Initial Rate of water absorption and days of curing in water.

Table 7
Secondary rate of water absorption for admixed concrete (x 10^{-6} m/$s^{0.5}$).

mix	days of curing					
	3	7	28	60	90	365
R0	1.21	1.15	0.91	0.76	0.62	0.59
M1	0.99	0.94	0.88	0.75	0.56	0.44
M2	0.60	0.55	0.53	0.51	0.47	0.43
R2	0.57	0.52	0.50	0.49	0.43	0.39
M3	0.51	0.50	0.47	0.43	0.43	0.37
R1M2	0.50	0.49	0.45	0.41	0.40	0.34
R1M3	1.21	1.15	0.91	0.76	0.62	0.59
M4	0.99	0.94	0.88	0.75	0.56	0.44
R2M2	0.60	0.55	0.53	0.51	0.47	0.43
R2M3	0.57	0.52	0.50	0.49	0.43	0.39

factor (R^2) as shown in Table 10.

One common linear equation between the secondary rate of water absorption ('y' in 10^{-6} m/$s^{0.5}$) and the initial rate of water absorption ('x' in 10^{-6} m/$s^{0.5}$) was developed by regression analysis (for all the mix)

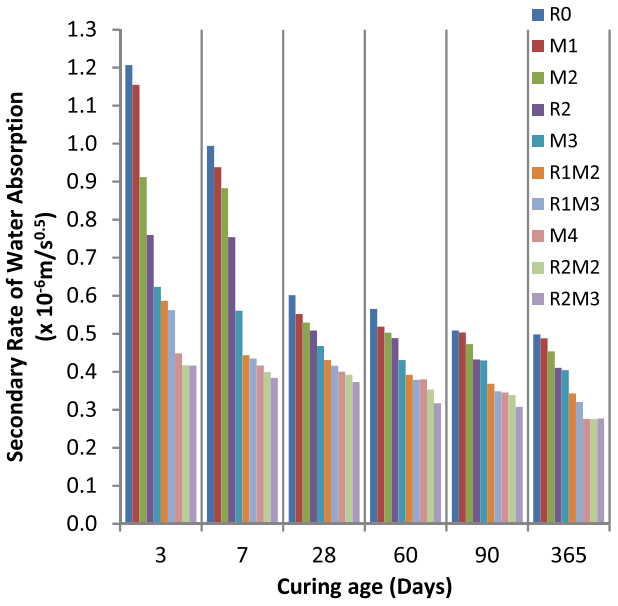

Fig. 7. Graph between Secondary Rate of water absorption and the days of curing in water.

with very high correlation factor (R^2) as shown in Table 11.

3.5. Coefficient of water absorption

The coefficient of water absorption of admixed concrete after 3, 7, 28, 60, 90 and 365 days of curing is given in Table 12 and shown in Fig. 8. The results were similar to that of the rate of water absorption test and the saturated water absorption test. The rate of change in the coefficient of water absorption of concrete for every mix designation was higher in the early days of curing in water (until 28 days). Thereafter, at later days of curing, the rate of change in the coefficient of water absorption nearly becomes constant. Thus it can be deduced that the later days of curing did not affect the coefficient of water absorption of admixed concrete as much as the early days of curing did. There was a significant reduction in the coefficient of water absorption of concrete of every mix designation as compared to concrete mix R0. The coefficient of water absorption of concrete was lowest for mix designation R2M3. The percentage decrease in the coefficient of water absorption of concrete for mix designation R2M3 as compared to R0 was 74%, 78%, 87%, 89%, 87% and 89% at 3, 7, 28, 60, 90 and 365 days of curing respectively. While the same for the mix designation M1 was 6%, 0%, 32%, 32%, 20% and 22% at 3, 7, 28, 60, 90 and 365 days of curing respectively. It confirms that the addition of MS and RSA reduces the coefficient of water absorption of concrete significantly because their addition leads to the densification of the concrete matrix and improvement in the ITZ.

The power equations between the coefficient of water absorption ('y' in 10^{-10} m^2/s) and days of curing in water ('x') were developed by regression analysis with high correlation factor (R^2) as shown in Table 13.

3.6. Chloride ion penetration

The chloride ion percentages at a depth of 10–20 mm and 25–35 mm for every mix designation are given in Table 14, Fig. 9 and Table 15, Fig. 10 respectively. The chloride percentage in concrete decreases with an increase in days of curing. The chloride percentage was higher at a depth of 10–20 mm as compared to the depth of 25–35 mm in concrete specimens at each day of curing. At 10–20 mm depth, the decrease in chloride percentage up to 28 days of curing was higher as compared to the decrease in chloride percentage beyond 28 days of curing. At 10–20 mm depth, the reduction in chloride percentage at 28 days of curing w.r.t. 7 days of curing of mix designation R0, M1, M2, R2, M3, R1M2, R1M3, M4, R2M2 and R2M3 was 48%, 47%, 46%, 45%, 48%, 47%, 44%, 45%, 35% and 23% respectively. Subsequently, the reduction in chloride percentage at 60 days of curing w.r.t. 28 days of curing was 2%, 2%, 13%, 12%, 6%, 3%, 3%, 1%, 8% and 11% respectively. Therefore it can be said that the chloride percentage at 10–20 mm depth was not affected by the curing age beyond 28 days and remained nearly constant after 28 days of curing. At 10–20 mm depth, the chloride ion percentage in the concrete of mix designation R2M3 was lowest at all the days of curing. At 10–20 mm depth, the chloride percentage in R2M3 w.r.t the control mix R0 was 36.87%, 60.73%, 42.06%, 47.53%, 67.15% and 78.94% after 3, 7, 28, 60, 90 and 365 days of curing in water respectively.

The result of chloride ion percentage at 25–35 mm depth was similar

Table 8
Mathematical relation between the initial rate of water absorption and curing age.

mix designation	mathematical equation	R^2
R0	$y = 14.089x^{-0.206}$	0.8689
M1	$y = 13.045x^{-0.194}$	0.8511
M2	$y = 13.155x^{-0.204}$	0.8696
R2	$y = 11.401x^{-0.183}$	0.8935
M3	$y = 9.6023x^{-0.151}$	0.9008
R1M2	$y = 9.4646x^{-0.155}$	0.9304
R1M3	$y = 7.9986x^{-0.122}$	0.9649
M4	$y = 7.6106x^{-0.118}$	0.9669
R2M2	$y = 6.2511x^{-0.085}$	0.8401
R2M3	$y = 6.0423x^{-0.123}$	0.9689

Table 9
Mathematical relation between the secondary rate of water absorption and curing age.

mix designation	mathematical equation	R^2
R0	$y = 1.3825x^{-0.202}$	0.8874
M1	$y = 1.2867x^{-0.196}$	0.8513
M2	$y = 1.0801x^{-0.17}$	0.8707
R2	$y = 0.9069x^{-0.148}$	0.917
M3	$y = 0.6673x^{-0.095}$	0.939
R1M2	$y = 0.5983x^{-0.101}$	0.8802
R1M3	$y = 0.5871x^{-0.108}$	0.9162
M4	$y = 0.5149x^{-0.092}$	0.8813
R2M2	$y = 0.4767x^{-0.081}$	0.8739
R2M3	$y = 0.463x^{-0.087}$	0.9454

Table 10
Mathematical relation between the secondary and initial rate of water absorption.

mix designation	mathematical equation	R^2
R0	$y = 0.0955x + 0.0267$	0.9992
M1	$y = 0.0997x - 0.0104$	0.997
M2	$y = 0.0729x + 0.1228$	0.9793
R2	$y = 0.0687x + 0.1229$	0.9902
M3	$y = 0.0491x + 0.1979$	0.9486
R1M2	$y = 0.0451x + 0.1694$	0.766
R1M3	$y = 0.0674x + 0.050$	0.8876
M4	$y = 0.0498x + 0.1215$	0.8322
R2M2	$y = 0.0693x + 0.037$	0.9423
R2M3	$y = 0.0581x + 0.1125$	0.93

Table 11
Mathematical relation between the secondary and initial rate of water absorption for all the mix.

mathematical equation	R^2
$y = 0.0892x - 0.02$	0.8791

Table 12
Coefficient of water absorption (x 10^{-10} m^2/s).

curing age, days	mix designation									
	R0	M1	M2	R2	M3	R1M2	R1M3	M4	R2M2	R2M3
3	8.22	7.75	7.57	6.37	4	3.18	2.83	2.72	2.48	2.12
7	7.43	7.43	4.7	4	3.02	2.55	2.32	1.86	1.82	1.62
28	6.4	4.38	2.36	2.01	1.85	1.68	1.52	1.44	1.4	0.84
60	5.66	3.87	2.13	1.85	1.57	1.39	1.26	1.25	1.14	0.61
90	4.58	3.64	1.88	1.5	1.48	1.23	1.06	1.07	0.84	0.57
365	4.4	3.43	1.73	1.35	1.3	1.07	0.9	0.88	0.67	0.46

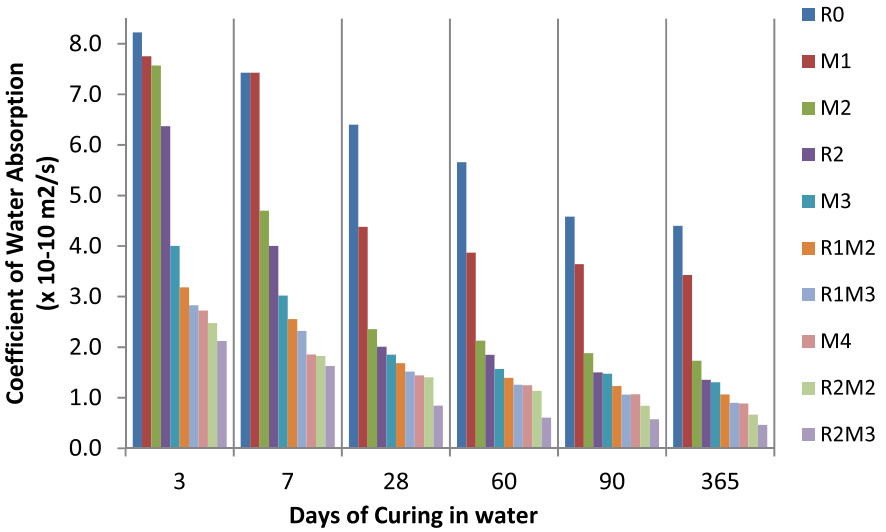

Fig. 8. Graph between Days of curing & Coefficient of water absorption.

Table 13
Mathematical relation between the coefficient of water absorption and days of curing.

mix designation	mathematical equation	R^2
R0	$y = 9.7027x^{-0.14}$	0.9391
M1	$y = 9.5402x^{-0.198}$	0.8996
M2	$y = 8.733x^{-0.318}$	0.8883
R2	$y = 7.6635x^{-0.333}$	0.9144
M3	$y = 4.7468x^{-0.246}$	0.9349
R1M2	$y = 3.9606x^{-0.241}$	0.9697
R1M3	$y = 3.651x^{-0.253}$	0.9782
M4	$y = 3.1543x^{-0.227}$	0.9664
R2M2	$y = 3.2817x^{-0.275}$	0.9766
R2M3	$y = 2.9015x^{-0.342}$	0.9534

Table 14
Percentage of chloride ion at 10–20 mm depth.

mix	days of curing					
	3	7	28	60	90	365
R0	1.406	1.350	0.708	0.693	0.687	0.678
M1	1.299	1.283	0.676	0.664	0.652	0.646
M2	1.242	1.225	0.666	0.579	0.560	0.559
R2	1.202	1.159	0.636	0.561	0.544	0.537
M3	1.163	1.122	0.580	0.545	0.505	0.489
R1M2	1.126	0.863	0.457	0.445	0.430	0.428
R1M3	1.021	0.790	0.440	0.425	0.422	0.405
M4	0.977	0.764	0.421	0.416	0.400	0.261
R2M2	0.945	0.648	0.419	0.387	0.242	0.180
R2M3	0.888	0.530	0.410	0.364	0.226	0.143

to the chloride ion percentage at 10–20 mm depth. At 25–35 mm depth, the decrease in chloride percentage up to 28 days of curing was higher as compared to the decrease in chloride percentage beyond 28 days of curing. At 25–35 mm depth, the reduction in chloride percentage at 28 days of curing w.r.t. 7 days of curing of mix designation R0, M1, M2, R2, M3, R1M2, R1M3, M4, R2M2 and R2M3 was 47%, 46%, 45%, 43%, 47%, 46%, 45%, 43%, 24% and 23% respectively. Subsequently, the decrease in chloride percentage at 60 days of curing w.r.t. 28 days of curing was 4%, 13%, 12%, 14%, 2%, 3%, 1%, 6%, 7% and 11% respectively. Therefore, it can be said that the chloride percentage at 25–35 mm depth was not affected by the curing age beyond 28 days and remained nearly constant after 28 days of curing. Concrete mix R2M3 had the least percentage of chloride ion at 25–35 mm depth. At 25–35 mm depth, the chloride percentage in R2M3 w.r.t. control mix R0 was 39.38%, 62.29%, 45.81%, 47.65%, 66.93% and 75.08% after 3, 7, 28, 60, 90 and 365 days of curing in water respectively.

The higher resistance to the penetration of chloride ions into the admixed concrete was due to the densification of its pore structure by the fine particles of RSA and MS [13]. As per the literature, the higher resistance could also be due to the improved interfacial transition zone (ITZ) around the aggregates [43]. As the microsilica and rice straw ash particles were finer than the OPC particles, they filled up the micro and macro pores of the concrete completely [44]. Microsilica and rice straw ash fill the voids of the hydrated cement paste, thereby decreasing the permeability of concrete [31]. Thus, it can be concluded that the microsilica and rice straw ash increases the resistance of the concrete to chloride ion penetration.

The power equations between the chloride percentage at both depths ('y') and days of curing ('x') were developed by regression analysis with high correlation factor (R^2) as shown in Tables 16 and 17.

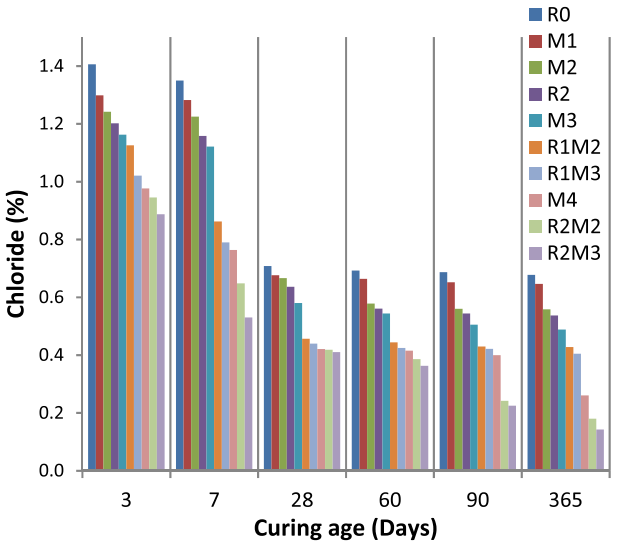

Fig. 9. Graph showing the percentage of chloride ion at 10–20 mm depth w.r.t Days of curing in water.

Table 15
Percentage of chloride ion at 25–35 mm depth.

mix	days of curing					
	3	7	28	60	90	365
R0	1.362	1.307	0.689	0.664	0.652	0.646
M1	1.258	1.242	0.666	0.582	0.578	0.573
M2	1.242	1.186	0.648	0.571	0.548	0.547
R2	1.202	1.122	0.636	0.545	0.527	0.499
M3	1.126	1.021	0.546	0.537	0.505	0.489
R1M2	1.065	0.820	0.442	0.427	0.425	0.405
R1M3	0.988	0.765	0.423	0.419	0.410	0.277
M4	0.953	0.740	0.419	0.394	0.381	0.237
R2M2	0.917	0.548	0.415	0.386	0.240	0.179
R2M3	0.799	0.477	0.369	0.327	0.203	0.128

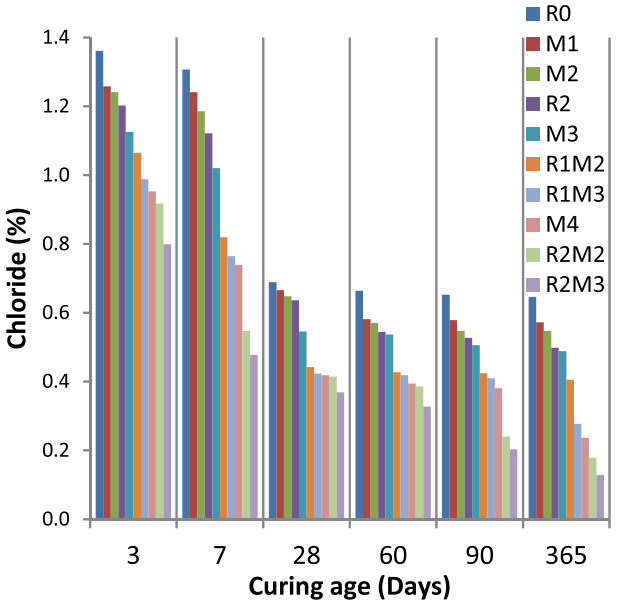

Fig. 10. Graph showing the percentage of chloride ion at 25–35 mm depth w.r.t Days of curing in water.

Table 16
Mathematical relation between chloride percentage at 10–20 mm depth and days of curing.

mix designation	mathematical equation	R^2
R0	$y = 1.6326x^{-0.181}$	0.7886
M1	$y = 1.5202x^{-0.176}$	0.7854
M2	$y = 1.5258x^{-0.203}$	0.8416
R2	$y = 1.4592x^{-0.201}$	0.8479
M3	$y = 1.4323x^{-0.213}$	0.8566
R1M2	$y = 1.2327x^{-0.219}$	0.8109
R1M3	$y = 1.1152x^{-0.207}$	0.8248
M4	$y = 1.2497x^{-0.27}$	0.9611
R2M2	$y = 1.3326x^{-0.344}$	0.9683
R2M3	$y = 1.255x^{-0.357}$	0.9507

Table 17
Mathematical relation between chloride percentage at 25–35 mm depth and days of curing.

mix designation	mathematical equation	R^2
R0	$y = 1.5928x^{-0.185}$	0.8
M1	$y = 1.533x^{-0.2}$	0.8288
M2	$y = 1.5057x^{-0.204}$	0.8464
R2	$y = 1.4785x^{-0.213}$	0.8879
M3	$y = 1.3171x^{-0.198}$	0.8426
R1M2	$y = 1.1717x^{-0.216}$	0.8255
R1M3	$y = 1.2316x^{-0.26}$	0.9566
M4	$y = 1.2546x^{-0.284}$	0.9744
R2M2	$y = 1.1968x^{-0.323}$	0.9455
R2M3	$y = 1.1295x^{-0.357}$	0.9577

Table 18
Mathematical relation between chloride percentage at 25–35 mm depth and 10–20 mm depth.

mix designation	mathematical equation	R^2
R0	$y = 0.9779x - 0.0132$	0.9998
M1	$y = 1.032x - 0.0815$	0.9941
M2	$y = 0.9887x - 0.0057$	0.9985
R2	$y = 1.0045x - 0.0216$	0.9972
M3	$y = 0.9043x + 0.0403$	0.9933
R1M2	$y = 0.9338x + 0.0141$	0.9995
R1M3	$y = 1.0259x - 0.0519$	0.9723
M4	$y = 0.9907x - 0.0142$	0.9991
R2M2	$y = 0.9246x + 0.0128$	0.9842
R2M3	$y = 0.9x - 2*10^{-16}$	1

The linear equations between the percentage of chloride ion at 25–35 mm depth ('y') and at 10–20 mm depth ('x') were developed by regression analysis for every mix designation with high correlation factor (R^2) as shown in Table 18.

One common linear equation between the percentage of chloride ion at 25–35 mm depth ('y') and at 10–20 mm depth ('x') was developed for all the mix as shown in Table 19.

3.7. Predictive graphs

The regression equations between the age of curing and saturated water absorption (Table 5), the rate of water absorption (Tables 8 and 9),

Table 19
Mathematical relation between chloride percentage at 25–35 mm and 10–20 mm depth for all mix.

mathematical equation	R^2
y = 0.976x - 0.0137	0.9928

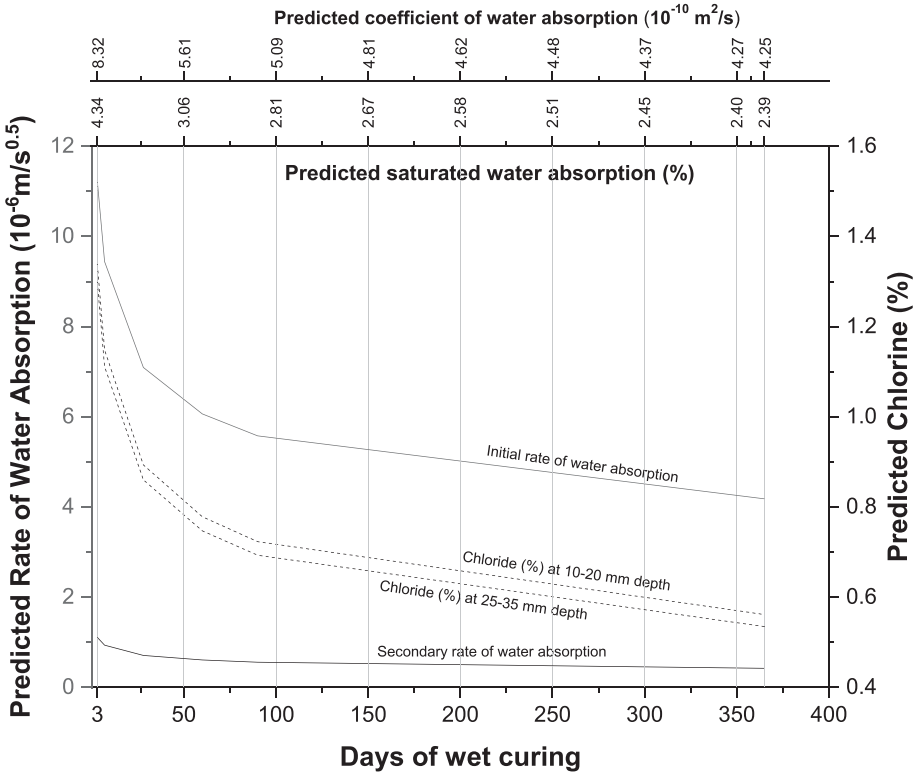

a) R0

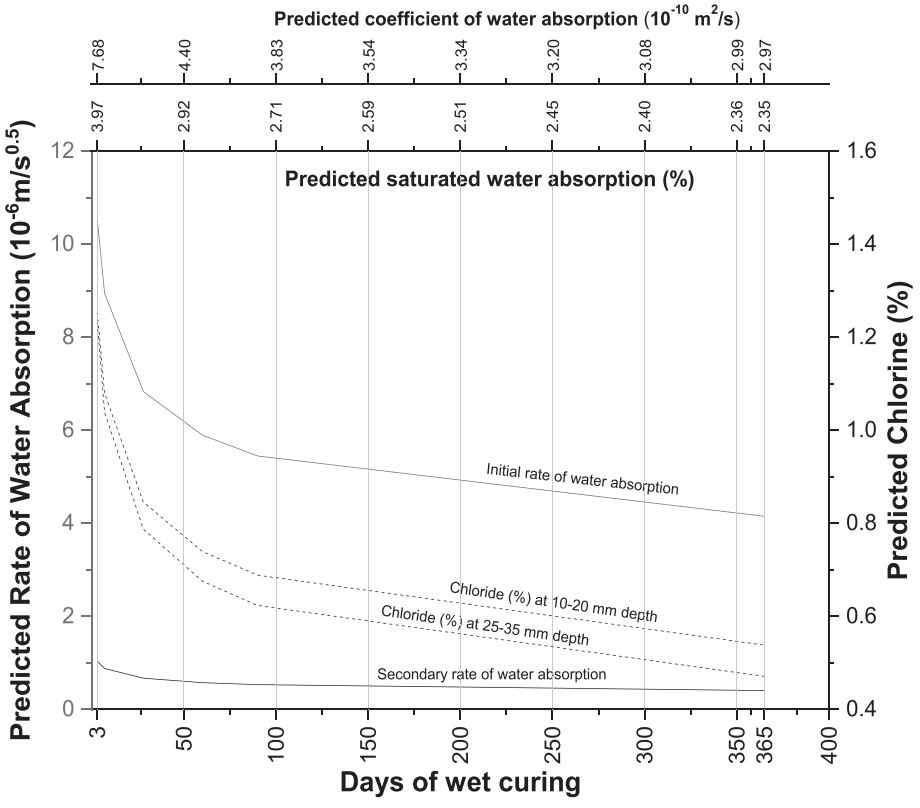

b) M1

Fig. 11. Predictive charts of the various mix for M40 grade PQC (a) R0 (b) M1 (c) M2 (d) R2 (e) M3 (f) R1M2 (g) R1M3 (h) M4 (i) R2M2 (j) R2M3.

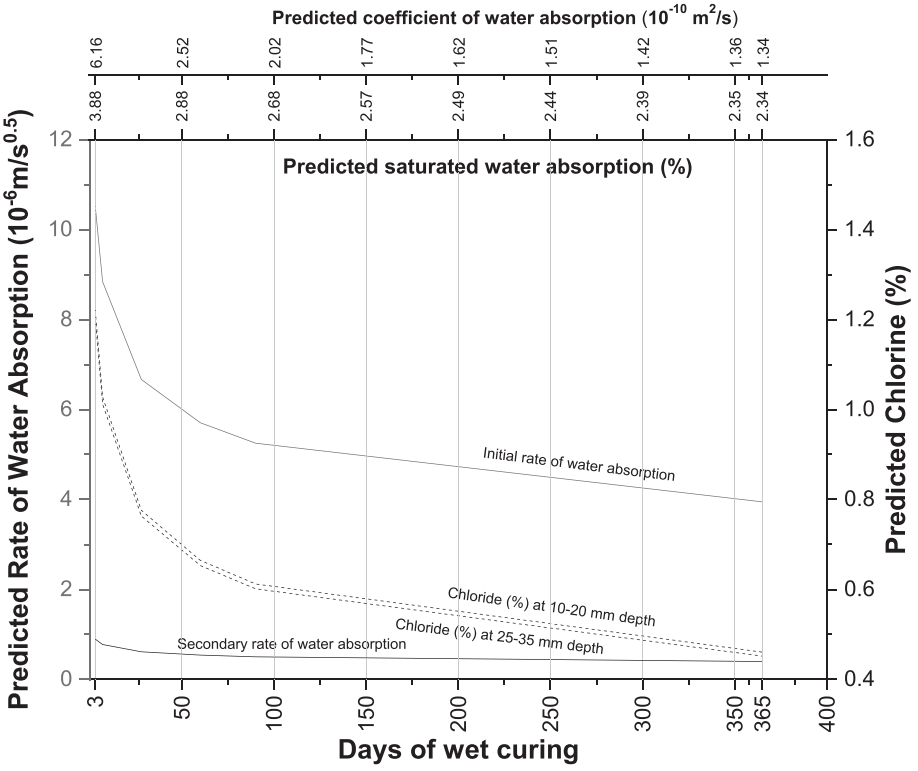

c) M2

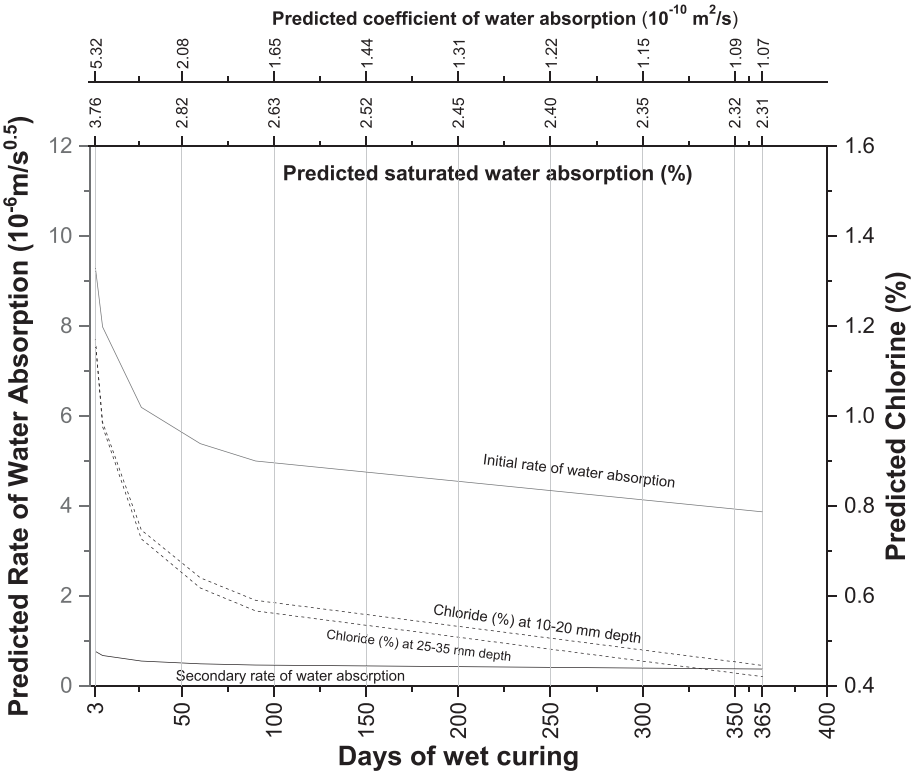

d) R2

Fig. 11. (*continued*).

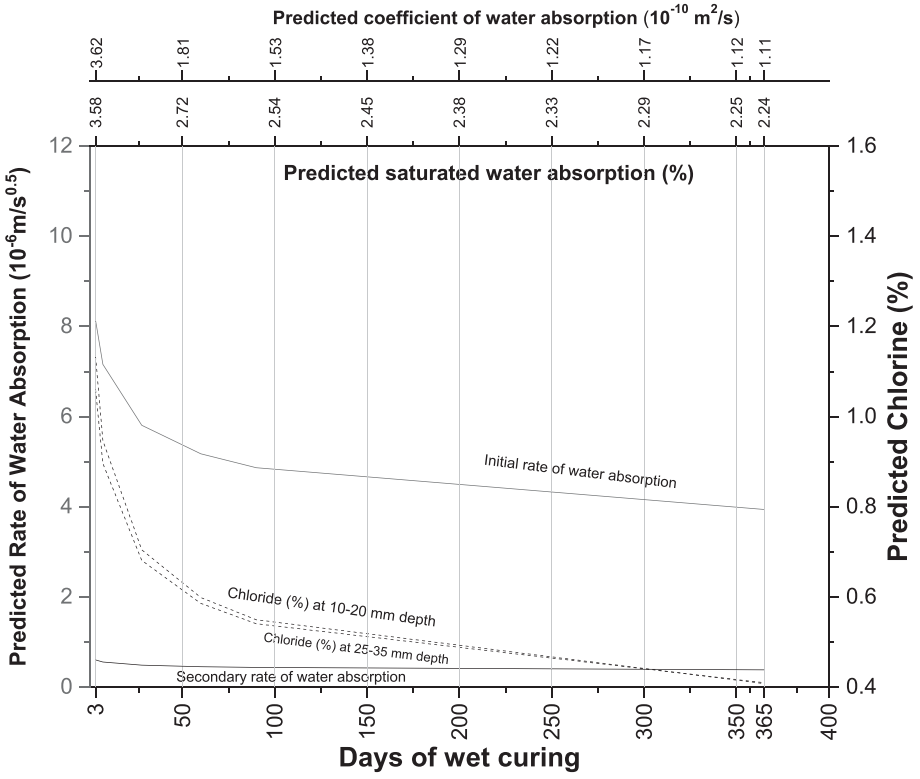

e) M3

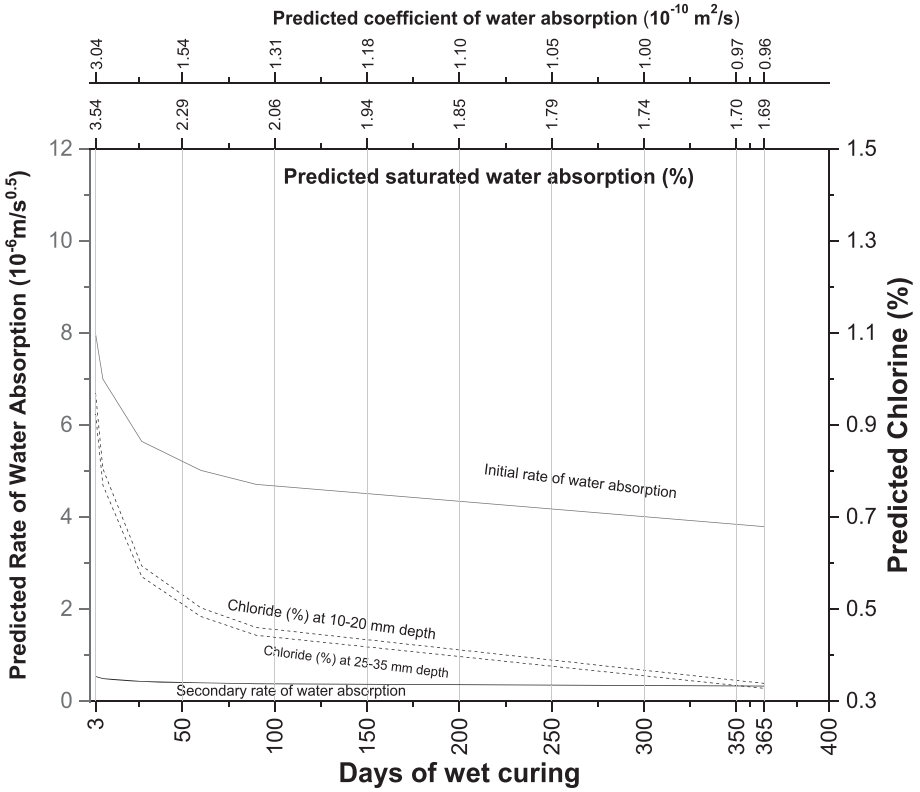

f) R1M2

Fig. 11. (*continued*).

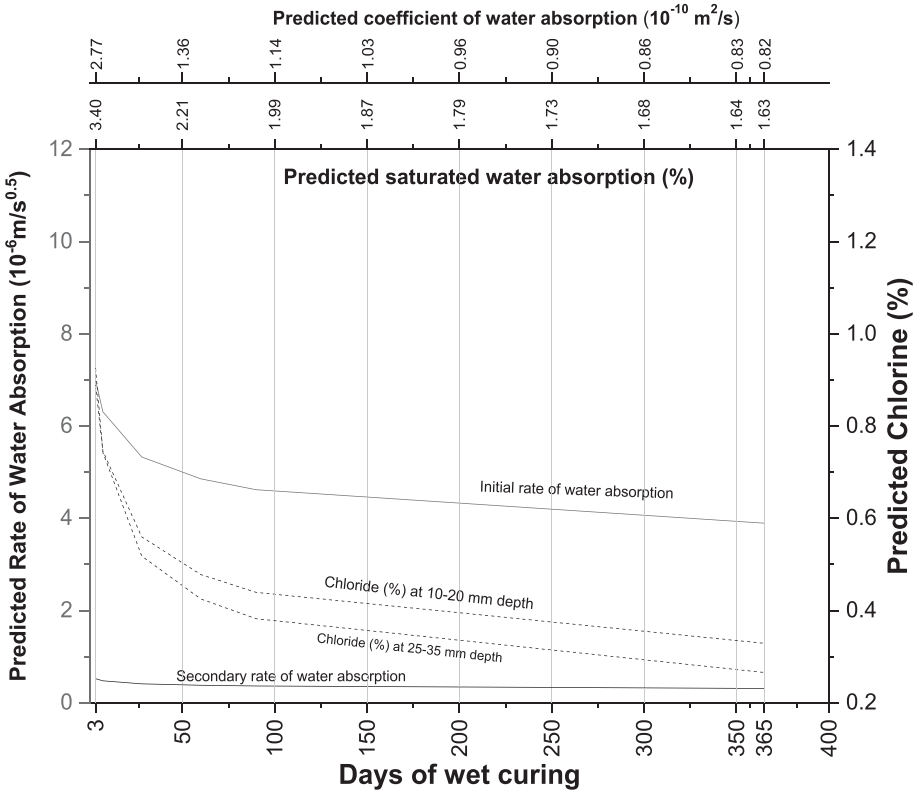

g) R1M3

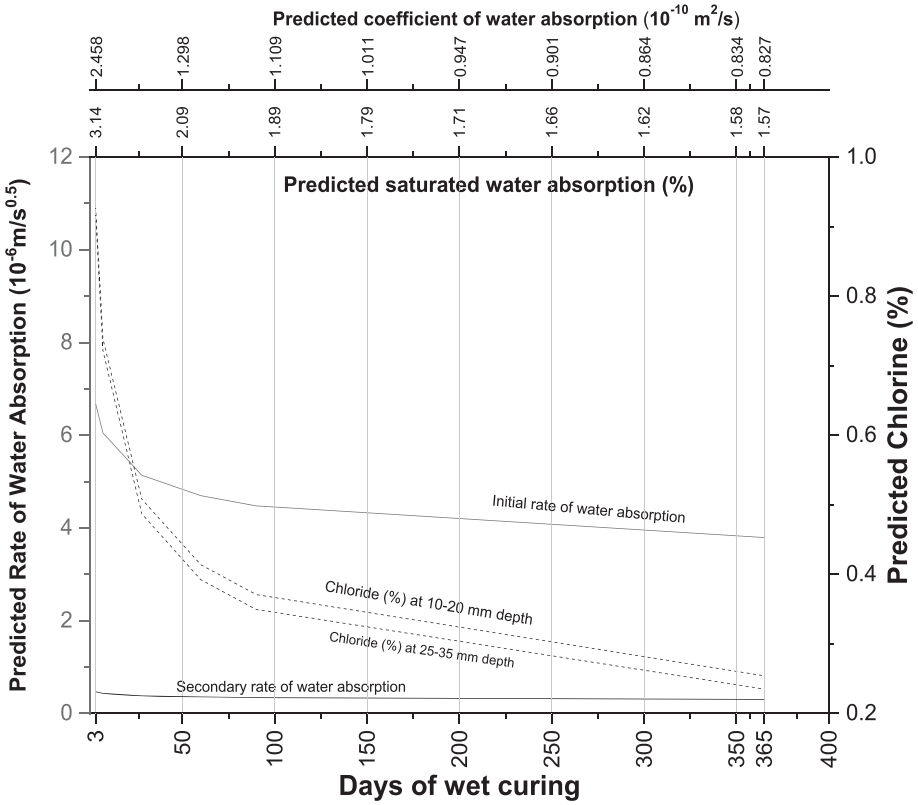

h) M4

Fig. 11. (*continued*).

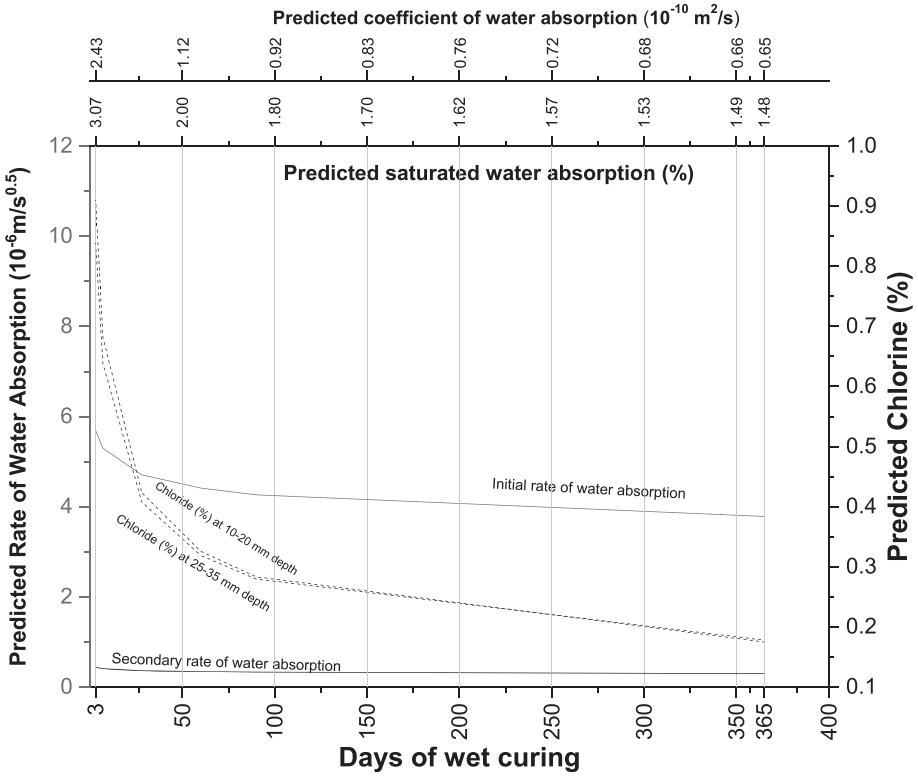

i) R2M2

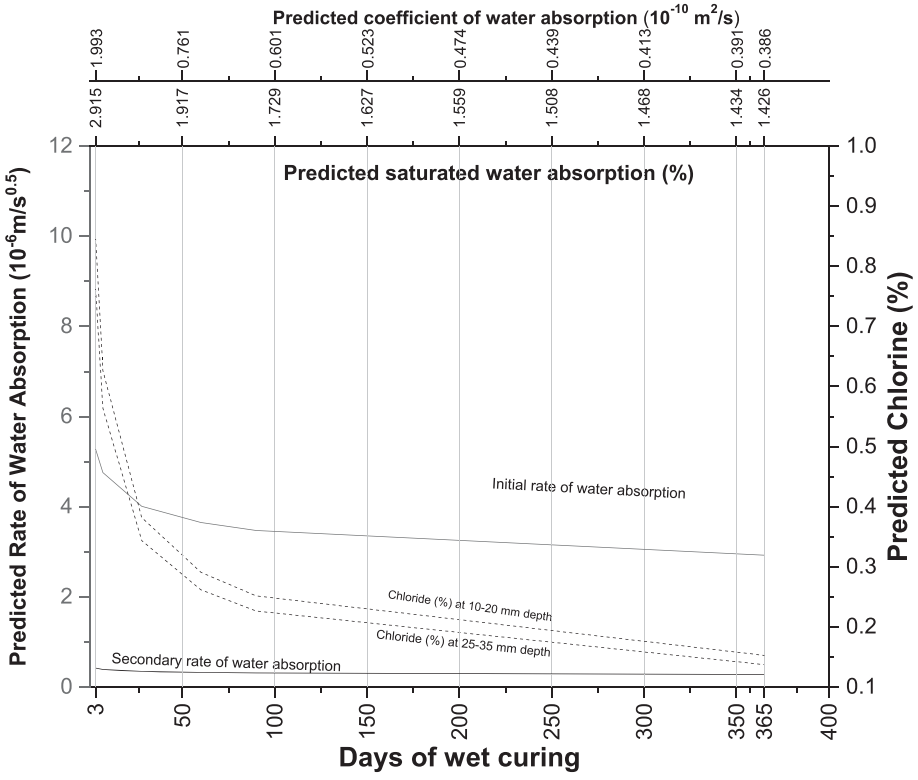

j) R2M3

Fig. 11. (*continued*).

the coefficient of water absorption (Table 13) and chloride ion penetration (Tables 16 and 17) were generated using the experimental readings. Based on the equations developed, the saturated water absorption, the initial and secondary rate of water absorption, the coefficient of water absorption and chloride ion penetration at depth 10–20 mm and 25–35 mm were again predicted from the days of curing. The predictive graphs were then plotted between the predicted parameters and days of water curing, as can be seen in Fig. 11.

4. Conclusion

It is a well-known fact that microsilica imparts significant improvement to various properties of the concrete by densifying the matrix [2, 4, 31, 45]. However, microsilica is a costly material. Thus a material was needed, which is economical as well as which imparts improvement in the durability properties of the concrete. It was found in the previous study that rice straw had both the features [7]. Following conclusions can be drawn from tests done in this investigation:

- RSA and MS particles were 5 and 28 times finer than the OPC particles, respectively.
- If w/b ratio is kept constant, the amount of microsilica and rice straw ash in the concrete significantly affects the air content of the fresh concrete. When 15% or more cement was replaced by microsilica and rice straw ash, the air content of the fresh concrete became constant.
- The addition of microsilica and rice straw ash decreases the saturated water absorption of admixed concrete. Concrete of mix designation R2M3 had the lowest saturated water absorption amongst all the concrete mix. The saturated water absorption was lower for MS admixed concrete as compared to the RSA admixed concrete.
- The initial rate of water absorption of concrete for every mix designation was constant when subjected to more than 28 days of curing. The secondary rate of water absorption of concrete for the mix designation R1M2, R1M3, M4, R2M2, and R2M3 was constant when subjected to water curing beyond 28 days. While for the mix designation R0, M1, M2, R2, and M3, the secondary rate of water absorption was constant when subjected to water curing beyond 7 days. The lowest rate of water absorption in concrete was observed for mix designation R2M3. A common linear equation between initial (x) and secondary (y) rate of water absorption in admixed concrete was developed ($y = 0.0892x - 0.02$, $R^2 = 0.8791$).
- A significant decrease in the coefficient of water absorption in the concrete of every mix designation was observed when compared with the control concrete R0. The highest and lowest coefficient of water absorption in concrete w.r.t. control concrete R0 was observed for mix designation M1 and R2M3, respectively.
- The higher resistance of admixed concrete to water absorption as compared to control concrete confirms that the volume of pore space reduces with the admixing of MS and RSA.
- With an increase in the curing age, there is a significant improvement in the defence mechanism of the admixed concrete to chloride ion penetration. The chloride percentage at 10–20 mm depth of concrete was more as compared to the 25–35 mm depth. For 10–20 mm and 25–35 mm depth, the chloride percentage in the concrete of every mix designation was constant when subjected to curing beyond 28 days. A common linear equation between chloride percentage at 10–20 mm depth (x in %) and 25–35 mm depth (y in %) was developed ($y = 0.976x - 0.0137$, $R^2 = 0.9928$).
- Various equations were developed based on experimental values between various parameters studied. These equations may help in anticipating one parameter from another without gathering the information. The only drawback was that they would work only for RSA and MS admixed concrete at $w/b = 0.39$. The proposed equations, whether applicable to admixing of different materials in concrete with different w/b ratio is a matter of future research.
- Predictive graphs were generated using the equations shown in Tables 5, 8, 9, 13, 16, and 17 for predicting water absorption and chloride percentage from the age of curing. Although predicting future results are necessarily questionable, so exact data about what's to come is much of the time incomprehensible. But the forecast can be helpful in making arrangements about conceivable developments.
- By findings from this study, mix R2M3 is recommended for admixed concrete because of its higher resistance to water absorption and chloride ion penetration as compared to the other mixes.

Declarations

Author contribution statement

Arunabh Pandey: Conceived and designed the experiments; Performed the experiments; Analyzed and interpreted the data; Contributed reagents, materials, analysis tools or data; Wrote the paper.

Brind Kumar: Conceived and designed the experiments; Analyzed and interpreted the data.

Funding statement

This research did not receive any specific grant from funding agencies in the public, commercial, or not-for-profit sectors.

Competing interest statement

The authors declare no conflict of interest.

Additional information

No additional information is available for this paper.

References

[1] M. Madani Hosseini, Y. Shao, J.K. Whalen, Biocement production from silicon-rich plant residues: perspectives and future potential in Canada, Biosyst. Eng. 110 (2011) 351–362.
[2] A.S. Baid, S.D. Bhole, Effect of Silica fume on mechanical properties of Concrete, Int. J. Eng. Res. Technol. 2 (2013) 230–238.
[3] G.D. Ransinchung, B. Kumar, Investigations on pastes and mortars of ordinary Portland cement admixed with wollastonite and microsilica, J. Mater. Civ. Eng. 22 (2009) 305–313.
[4] S. Singh, G.D. Ransinchung, P. Kumar, Effect of mineral admixtures on fresh, mechanical and durability properties of RAP inclusive concrete, Constr. Build. Mater. 156 (2017) 19–27.
[5] IARI, Crop Residues Management with Conservation Agriculture: Potential, Constraints and Policy Needs, Indian Agricultural Research Institute, 2012 vii+32 p.
[6] N.H. Ravindranath, H.I. Somashekar, M.S. Nagaraja, P. Sudha, G. Sangeetha, S.C. Bhattacharya, P. Abdul Salam, Assessment of sustainable non-plantation biomass resources potential for energy in India, Biomass Bioenergy 29 (2005) 178–190.
[7] A. Pandey, B. Kumar, Analysis of rice straw ash for part replacement of OPC in pavement quality concrete, in: International Conference on Civil and Environmental Engineering, Singapore, 2016.
[8] M.A. El-Sayed, T.M. El-Samni, Physical and chemical properties of rice straw ash and its effect on the cement paste produced from different cement types, J. Eng. Sci. King Saud Univ. 19 (2006) 21–29.
[9] S. Munshi, G. Dey, R. Prasad Sharma, Use of rice straw ash as pozzolanic material in cement mortar, Int. J. Eng. Technol. 5 (2013) 603–606.
[10] A. Pandey, B. Kumar, Preliminary study of cement paste admixed with rice straw ash, microsilica & rice straw ash-microsilica composite, Int. J. Recent Technol. Eng. 7 (2019) 302–307.
[11] J. Roselló, L. Soriano, M.P. Santamarina, J.L. Akasaki, J. Monzó, J. Payá, Rice straw ash: a potential pozzolanic supplementary material for cementing systems, Ind. Crops Prod. 103 (2017) 39–50.
[12] S. Munshi, R.P. Sharma, Experimental investigation on strength and water permeability of mortar incorporate with rice straw ash, Adv. Mater. Sci. Eng. 2016 (2016) 1–7.
[13] A.A. Ramezanianpour, V.M. Malhotra, Effect of curing on the compressive strength, resistance to chloride-ion penetration and porosity of concretes incorporating slag, fly ash or silica fume, Cement Concr. Compos. 17 (1995) 125–133.

[14] L.P. Singh, A. Goel, S.K. Bhattacharyya, G. Mishra, Quantification of hydration products in cementitious materials incorporating silica nanoparticles, Front. Struct. Civ. Eng. 10 (2016) 162–167.
[15] M. Limbachiya, M.S. Meddah, Y. Ouchagour, Use of recycled concrete aggregate in fly-ash concrete, Constr. Build. Mater. 27 (2012) 439–449.
[16] D. Harbec, A. Zidol, A. Tagnit-Hamou, F. Gitzhofer, Mechanical and durability properties of high performance glass fume concrete and mortars, Constr. Build. Mater. 134 (2017) 142–156.
[17] A. Pandey, B. Kumar, Effects of rice straw ash and micro silica on mechanical properties of pavement quality concrete, J. Build. Eng. 26 (2019) 1–12.
[18] A. Pandey, B. Kumar, Investigating the performance of cement mortar containing rice straw ash , microsilica and their composite by compressive strength, Int. J. Recent Technol. Eng. 7 (2019) 91–94.
[19] IRC 44, Guidelines for Cement Concrete Mix Design for Pavements, Indian Road Congress, New Delhi, 2017.
[20] IS 10262, Concrete Mix Proportioning - Guidelines, Bureau of Indian Standards, New Delhi, 2009.
[21] ASTM C143, Standard Test Method for Slump of Hydraulic-Cement Concrete, ASTM International., 2015.
[22] ASTM C231/C231M, Standard Test Method for Air Content of Freshly Mixed Concrete by the Pressure Method, ASTM International, 2010.
[23] ASTM C192/C192M-16a, Standard Practice for Making and Curing Test Specimens in the Laboratory, ASTM International, 2016.
[24] ASTM C642-13, Standard Test Method for Density, Absorption, and Voids in Hardened concrete, ASTM International, 2013.
[25] ASTM C1585, Standard Test Method for Measurement of Rate of Absorption of Water by Hydraulic-Cement Concretes, ASTM International, 2013.
[26] ASTM C1543, Standard Test Method for Determining the Penetration of Chloride Ion into Concrete by Ponding, ASTM International, 1996.
[27] ASTM C1152/1152M, Standard Test Method for Acid-Soluble Chloride in Mortar and Concrete 1 ASTM, ASTM International, 2006, pp. 5–8, 15.
[28] ASTM C618-19, Standard Specification for Coal Fly Ash and Raw or Calcined Natural Pozzolan for Use, ASTM International., 2019.
[29] Y. Ruangtaweep, N. Srisittipokakun, K. Boonin, P. Yasaka, J. Kaewkhao, Characterization of rice straw ash and utilization in glass production, Adv. Mater. Res. 748 (2013) 304–308.
[30] R. Shamsudin, H. Ismail, M.A. Abdul Hamid, The suitability of rice straw ash as a precursor for synthesizing β-wollastonite, Mater. Sci. Forum 846 (2016) 216–222.
[31] G.D. Ransinchung, B. Kumar, V. Kumar, Assessment of water absorption and chloride ion penetration of pavement quality concrete admixed with wollastonite and microsilica, Constr. Build. Mater. 23 (2009) 1168–1177.
[32] N. Quaranta, M. Unsen, H. López, C. Giansiracusa, J.A. Roether, A.R. Boccaccini, Ash from sunflower husk as raw material for ceramic products, Ceram. Int. 37 (2011) 377–385.
[33] X. Yao, K. Xu, Y. Liang, Comparing the thermo-physical properties of rice husk and rice straw as feedstock for thermochemical conversion and characterization of their waste ashes from combustion, BioResources 11 (2016) 10549–10564.
[34] T. Gonçalves, R.V. Silva, J. de Brito, J.M. Fernández, A.R. Esquinas, Hydration of reactive MgO as partial cement replacement and its influence on the macroperformance of cementitious mortars, Adv. Mater. Sci. Eng. 2019 (2019) 1–12.
[35] L. Mo, M. Deng, A. Wang, Effects of MgO-based expansive additive on compensating the shrinkage of cement paste under non-wet curing conditions, Cement Concr. Compos. 34 (2012) 377–383.
[36] L. Mo, M. Deng, M. Tang, Effects of calcination condition on expansion property of MgO-type expansive agent used in cement-based materials, Cement Concr. Res. 40 (2010) 437–446.
[37] A. Kostrzanowska-Siedlarz, J. Gołaszewski, Rheological properties and the air content in fresh concrete for self compacting high performance concrete, Constr. Build. Mater. 94 (2015) 555–564.
[38] S. Kosmatka, Control of air content in concrete, Portland Cement Assoc. 19 (1998) 1–8.
[39] D. Whiting, D. Stark, NCHRP 258, Control of Air Content in Concrete, Transport Research Board, 1983.
[40] P. Duan, Z. Shui, W. Chen, C. Shen, Effects of metakaolin, silica fume and slag on pore structure, interfacial transition zone and compressive strength of concrete, Constr. Build. Mater. 44 (2013) 1–6.
[41] B. Liu, G. Luo, Y. Xie, Effect of curing conditions on the permeability of concrete with high volume mineral admixtures, Constr. Build. Mater. 167 (2018) 359–371.
[42] A. Kotwa, Effect of selected admixtures on the properties of ordinary concrete, Proc. Eng. 108 (2015) 504–509.
[43] M.A. Glinicki, D. Jóźwiak-Niedźwiedzka, K. Gibas, M. Dabrowski, Influence of blended cements with calcareous fly ash on chloride ion migration and carbonation resistance of concrete for durable structures, Materials 9 (2016).
[44] K. Ganesan, K. Rajagopal, K. Thangavel, Evaluation of bagasse ash as supplementary cementitious material, Cement Concr. Compos. 29 (2007) 515–524.
[45] S. Singh, G.D.R.N. Ransinchung, K. Monu, P. Kumar, Laboratory investigation of RAP aggregates for dry lean concrete mixes, Constr. Build. Mater. 166 (2018) 808–816.